Springer

Journal of Mechanical Science and Technology 23 (2009) 1508~1514

Journal of Mechanical Science and Technology

www.springerlink.com/content/1738-494x
DOI 10.1007/s12206-009-0404-6

Elastic stresses and failure of rotating cross-ply laminate disks †

Kyo-Nam Koo*

Department of Aerospace Engineering, University of Ulsan, Ulsan, 680-749, Korea

(Manuscript Received February 26, 2008; Revised January 23, 2009; Accepted April 1, 2009)

Abstract

Centrifugal force acting on a rotating disk induces in-plane loads in the radial and circumferential directions. An application of fiber-reinforced composite materials to a rotating disk can satisfy the demand for increasing its rotating speed. However, previous researches have been confined to single lamina disks. In this paper, a stress analysis of rotating disks made of multidirectional laminates is performed. The Tsai-Wu failure criterion is applied to the strength analysis of the rotating laminate disks, from which the maximum allowable speeds are obtained. The cross-ply ratios providing the maximum allowable speeds are obtained for the glass/epoxy and carbon/epoxy cross-ply laminate disks with CD geometry.

Keywords: Composite; Cross-ply ratio; Failure analysis; Laminate; Maximum rotating speed; Rotating disk

1. Introduction

Rotating disks are widely used in data storage devices such as CD's, DVD's (digital versatile disks), and HD's (hard disks) as well as in traditional machines such as circular saws, turbines, and so on. Rotating speed of isotropic disks can be limited by problems related to strength and stability. For example, although the demand for higher data transfer rate in computers needs faster CD drives, the 52×(52 times the transfer rate of the original CD) is expected to be the last polycarbonate CD. This is because the 52× CD drive has a rotating speed which is over its lowest critical speed [1]. Koo [2] showed that the application of fiber-reinforced composite materials to CD could make the critical speeds increase effectively. Fiber-reinforced composite materials have a tailorability of strength and stiffness in addition to high specific strength and stiffness.

Since the problem of rotating disks was first treated in the early twentieth century, the solutions of the isotropic disks including variable thickness, variable density, and other cases can be found in most of the standard elasticity textbooks [3]. As the application of composite materials increased to various fields, many papers [3-7] dealt with the stresses of rotating polar orthotropic disks. Recently, the present author has applied fiber-reinforced composite materials to CD's and showed that the maximum allowable rotating speed for static strength could be increased by radial or circumferential reinforcement [8].

The previous researches were confined to single lamina disks in which fibers are unidirectional, i.e., in the radial or circumferential directions. However, a single lamina plate is rarely used in application since it is very weak in bending as well as extension along the transverse direction. The high strength of fiber cannot be utilized in a single lamina plate since matrix failure could occur at a low stress level. Matrix failure in a single lamina plate implies total failure of the disk. In this paper, a multidirectional laminate disk is proposed for rotating disks, of which closed-form solutions for stress distribution are found. The main purpose of this work is to derive the elastic stresses of laminate disks

† This paper was recommended for publication in revised form by Associate Editor Heoung Jae Chun

* Corresponding author. Tel.: +82 52 259 1261, Fax.: +82 52 259 1682
E-mail address: knkoo@mail.ulsan.ac.kr

rotating at a constant speed. As an application of the stress solutions, a failure analysis of rotating laminate disks is performed. The Tsai-Wu failure criterion is applied to determine the strength of a laminate disk, from which the maximum allowable speed is obtained. Numerical examples are given and discussed for GFRP (glass fiber reinforced plastic) and CFRP (carbon fiber reinforced plastic) cross-ply laminate disks with CD geometry.

2. Governing equations

A composite laminate can be composed of as many layers as needed, of which fiber orientations could be arbitrary. However, one of the simple ways to make up a composite laminate disk is to stack the radially reinforced and circumferentially reinforced laminae as shown in Fig. 1. Laminates containing plies oriented only at 0° and 90° are called cross-ply laminates. The stress-strain relations for the k-th layer, $\{\sigma\}_k = [Q]_k \{\varepsilon\}_k$ in a multidirectional laminate disk under a state of plane stress are

$$\begin{Bmatrix} \sigma_1 \\ \sigma_2 \\ \tau_{12} \end{Bmatrix}_k = \begin{bmatrix} Q_{11} & Q_{12} & 0 \\ Q_{12} & Q_{22} & 0 \\ 0 & 0 & Q_{66} \end{bmatrix}_k \begin{Bmatrix} \varepsilon_1 \\ \varepsilon_2 \\ \gamma_{12} \end{Bmatrix}_k \tag{1}$$

where the subscripts 1 and 2 denote the fiber and transverse directions, respectively; the components of the reduced stiffness matrix $[Q]_k$ are defined as

$$Q_{11} = \frac{E_1}{1-\nu_{12}\nu_{21}}, \quad Q_{12} = \frac{\nu_{12}E_2}{1-\nu_{12}\nu_{21}},$$
$$Q_{22} = \frac{E_2}{1-\nu_{12}\nu_{21}}, \quad Q_{66} = G_{12}. \tag{2}$$

Normally, the lamina principal axes (1, 2) do not coincide with the loading or reference axes. The stress-strain relations in Eq. (1) can be transformed into the disk body axes (r,θ) which are fixed on a rotating disk as shown in Fig. 2:

$$\begin{Bmatrix} \sigma_r \\ \sigma_\theta \\ \tau_{r\theta} \end{Bmatrix}_k = \begin{bmatrix} \overline{Q}_{rr} & \overline{Q}_{r\theta} & \overline{Q}_{rs} \\ \overline{Q}_{r\theta} & \overline{Q}_{\theta\theta} & \overline{Q}_{\theta s} \\ \overline{Q}_{rs} & \overline{Q}_{\theta s} & \overline{Q}_{ss} \end{bmatrix}_k \begin{Bmatrix} \varepsilon_r \\ \varepsilon_\theta \\ \gamma_{r\theta} \end{Bmatrix}_k \quad \text{or}$$
$$\{\sigma_{r\theta}\}_k = [\overline{Q}]_k \{\varepsilon_{r\theta}\}_k \tag{3}$$

where the transformed reduced stiffness matrix $[\overline{Q}]_k$

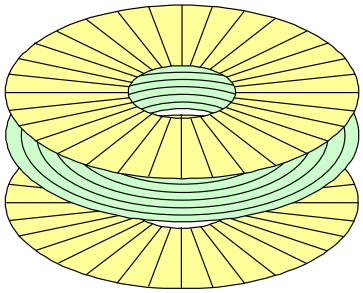

Fig. 1. Composite laminated disk.

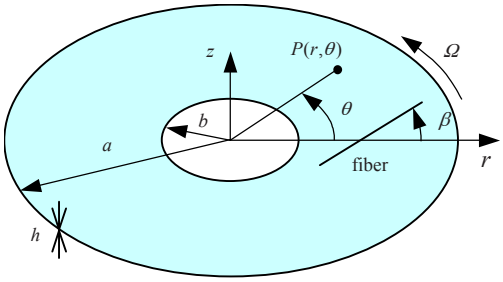

Fig. 2. Coordinates and geometry of rotating disk.

is obtained by

$$[\overline{Q}]_k = [T]_k^{-1}[Q]_k[T]_k^{-T}. \tag{4}$$

The transformation matrix $[T]_k$ in Eq. (4) is defined for the fiber orientation angle β measured positive counterclockwise from the r-axis to the fiber direction as shown in Fig. 2:

$$[T]_k = \begin{bmatrix} m^2 & n^2 & 2mn \\ n^2 & m^2 & -2mn \\ -mn & mn & m^2-n^2 \end{bmatrix} \tag{5}$$

where $m = \cos\beta$ and $n = \sin\beta$.

The in-plane force resultants N_r, N_θ, $N_{r\theta}$ for symmetric laminate are obtained by integrating the stresses in Eq. (3) through the thickness h:

$$\begin{Bmatrix} N_r \\ N_\theta \\ N_{r\theta} \end{Bmatrix} = \begin{bmatrix} A_{rr} & A_{r\theta} & A_{rs} \\ A_{r\theta} & A_{\theta\theta} & A_{\theta s} \\ A_{rs} & A_{\theta s} & A_{ss} \end{bmatrix} \begin{Bmatrix} \varepsilon_r \\ \varepsilon_\theta \\ \gamma_{r\theta} \end{Bmatrix} \tag{6}$$

where $[A]$ is the extensional stiffness matrix in a polar coordinate; and its components can be expressed by the thickness of the k-th layer t_k as

$$A_{ij} = \int_{-h/2}^{h/2} \overline{Q}_{ij} dz = \sum_{k=1}^{N} (\overline{Q}_{ij})_k t_k. \tag{7}$$

The strains due to the in-plane displacements u_r and u_θ in the radial and circumferential directions, respectively, can be written by

$$\varepsilon_r = \frac{\partial u_r}{\partial r}, \quad \varepsilon_\theta = \frac{1}{r}\left(u_r + \frac{\partial u_\theta}{\partial \theta}\right),$$
$$\gamma_{r\theta} = r\frac{\partial}{\partial r}\left(\frac{\partial u_\theta}{\partial r}\right) + \frac{\partial u_r}{r\partial \theta}. \tag{8}$$

Substituting the strains in Eq. (8) into Eq. (6), the force resultants for cross-ply symmetric laminate under axisymmetric deformation become

$$N_r = A_{rr}\frac{du_r}{dr} + A_{r\theta}\frac{u_r}{r}, \quad N_\theta = A_{r\theta}\frac{du_r}{dr} + A_{\theta\theta}\frac{u_r}{r},$$
$$N_{r\theta} = A_{ss}\left(\frac{du_\theta}{dr} - \frac{u_\theta}{r}\right) \tag{9}$$

where $N_{r\theta}$ vanishes when a disk rotates at a constant speed.

The force resultants N_r and N_θ produced by disk rotation can be determined from the equilibrium equation in the r-direction given by

$$-\frac{\partial}{\partial r}(rN_r) - \frac{\partial N_{r\theta}}{\partial \theta} + N_\theta = r(\rho h r \Omega^2) \tag{10}$$

where ρ is the density of a disk; and Ω is a rotating speed.

Along with $\partial N_{r\theta}/\partial\theta = 0$ for the axisymmetric situation, substituting the resultants in Eq. (9) into Eq. (10) yields the differential equation:

$$r^2\frac{d^2u_r}{dr^2} + r\frac{du_r}{dr} - \mu^2 u_r = -\frac{\rho h \Omega^2 r^3}{A_{rr}} \tag{11}$$

where $\mu^2 = A_{\theta\theta}/A_{rr}$.

3. Analytic solutions

Since the solution of Eq. (11) depends on the value of μ^2, we should consider two cases: $\mu^2 \neq 9$ and $\mu^2 = 9$. The general solution in case of $\mu^2 \neq 9$ could be written as

$$u_r(r) = c_1 r^\mu + c_2 r^{-\mu} - \frac{\rho h \Omega^2 r^3}{(9-\mu^2)A_{rr}}. \tag{12}$$

The coefficients c_1 and c_2 are determined by two boundary conditions, which are expressed for a disk fixed at inner radius b and free at outer radius a as follows:

$$u_r(b) = 0, \quad N_r(a) = 0. \tag{13}$$

The coefficients satisfying the boundary conditions are

$$c_1 = \frac{\rho h \Omega^2}{(9-\mu^2)A_{rr}}\frac{e}{d}, \quad c_2 = \frac{\rho h \Omega^2}{(9-\mu^2)A_{rr}}\frac{f}{d} \tag{14}$$

where

$$e = (3+\eta)a^3 b^{-\mu} + (\mu-\eta)a^{-\mu}b^3,$$
$$f = (\mu+\eta)a^\mu b^3 + (3+\eta)a^3 b^\mu,$$
$$d = (\mu+\eta)a^\mu b^{-\mu} + (\mu-\eta)a^{-\mu}b^\mu$$
$$\eta = A_{r\theta}/A_{rr}. \tag{15}$$

Substituting $u_r(r)$ in Eq. (12) into Eq. (9) yields

$$\frac{N_r}{\rho h \Omega^2} = c_{r1}r^{\mu-1} + c_{r2}r^{-\mu-1} - c_{r3}r^2$$
$$\frac{N_\theta}{\rho h \Omega^2} = c_{\theta 1}r^{\mu-1} + c_{\theta 2}r^{-\mu-1} - c_{\theta 3}r^2 \tag{16}$$

where

$$c_{r1} = \frac{\mu+\eta}{9-\mu^2}\frac{e}{d}, \quad c_{r2} = \frac{\mu-\eta}{9-\mu^2}\frac{f}{d}, \quad c_{r3} = \frac{3+\eta}{9-\mu^2},$$
$$c_{\theta 1} = \mu c_{r1}, \quad c_{\theta 2} = -\mu c_{r2}, \quad c_{\theta 3} = \frac{\mu^2+3\eta}{9-\mu^2}. \tag{17}$$

The solutions in case of $\mu^2 = 9$ are listed in Appendix. This case occurs when the modulus ratio E_1/E_2 of a single lamina disk equals nine but is not likely to occur in practice. Another case of $\mu^2 = 9$ occurs when the laminate $[0/90_9]_S$ is in the matrix failure in both 0° and 90° layers.

The in-plane normal strains of the cross-ply laminate disk in the body axes (r,θ) can be obtained from the following equation:

$$\begin{Bmatrix}\varepsilon_r \\ \varepsilon_\theta\end{Bmatrix} = \begin{bmatrix}A_{rr} & A_{r\theta} \\ A_{r\theta} & A_{\theta\theta}\end{bmatrix}^{-1}\begin{Bmatrix}N_r \\ N_\theta\end{Bmatrix}. \tag{18}$$

The shear strain $\gamma_{r\theta}$ vanishes when a disk rotates at a constant speed.

Since the in-plane strains are constant along the thickness direction, ε_1 and ε_2 in the k-th layer can be obtained just by transforming ε_r and ε_θ as follows:

$$\begin{Bmatrix}\varepsilon_1\\ \varepsilon_2\end{Bmatrix}_k = \begin{bmatrix}m^2 & n^2\\ n^2 & m^2\end{bmatrix}_k \begin{Bmatrix}\varepsilon_r\\ \varepsilon_\theta\end{Bmatrix}. \quad (19)$$

Finally, the stresses in each layer are determined by substituting the strains in Eq. (19) into Eq. (1).

4. Results and discussions

The rotating disks are assumed to have the same dimensions as those of CD media where b=15 mm, a=60 mm, h=1.2 mm. The three materials shown in Table 1 are selected to calculate the stress and failure analysis of the rotating laminate disks. The material properties of E-glass/Epoxy and T300/N5208 are used as typical properties of GFRP and CFRP, respectively. The strength constants in Table 1 are defined as

X_t = Longitudinal tensile strength

X_c = Longitudinal compressive strength

Y_t = Transverse tensile strength

Y_c = Transverse compressive strength

The stresses of $[0/90]_S$ GFRP and CFRP disks are plotted in Fig. 3 and Fig. 4, respectively, being compared with the finite element results obtained by using MSC/NASTRAN. The present analytic stresses are in very good agreement with the finite element results. Therefore, we can utilize the closed-form solution of stresses in a rotating laminate disk for strength analysis, vibration analysis, and so on.

Table 2 shows the maximum rotational speeds and failure modes for various disks based on the Tsai-Wu theory. The [0] disk is composed of layers oriented only in the radial direction; the [90] disk is composed of layers oriented only in the circumferential direction; the $[0/90]_S$ disk is composed of layers with equal thickness, oriented in the radial and circumferential directions, and symmetrically laminated about the mid plane.

In the failure analysis of laminate disks, two types of failures are discussed: (1) initial or first-ply failure (FPF) and (2) ultimate laminate failure (ULF). In this paper, matrix cracking or fiber breakage is regarded as failure of a lamina and the last fiber breakage as total failure of the laminate or ULF. The [0] and [90]

Table 1. Material properties.

Properties	Polycarbonate	GFRP	CFRP
E_1 (GPa)	2.2	38.6	181.0
E_2 (GPa)	2.2	8.27	10.3
G_{12} (GPa)	0.846	4.14	7.17
ν_{12}	0.38	0.26	0.28
ρ (kg/m^3)	1220	1800	1600
X_t (MPa)	64	1062	1500
X_c (MPa)	89	610	1500
Y_t (MPa)	64	31	40
Y_c (MPa)	89	118	246
S (MPa)	43	72	68

Table 2. Maximum rotating speeds.

Material		Max. speed (rpm)	Failure mode
Polycarbonate		51,876	Radial failure
GFRP	[0]	70,168	Matrix failure
	[90]	47,622	Matrix failure
	$[0/90]_S$	44,050 63,816 105,172	Matrix failure @ 90 Matrix failure@ 0 Fiber failure @ 0
CFRP	[0]	127,469	Fiber failure
	[90]	100,286	Matrix failure
	$[0/90]_S$	94,220 123,972	Matrix failure @ 90 Fiber failure @ 0

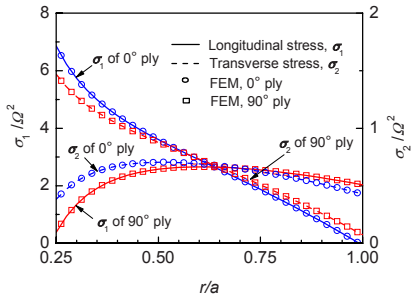

Fig. 3. Stresses in each layer of GFRP $[0/90]_S$ disk.

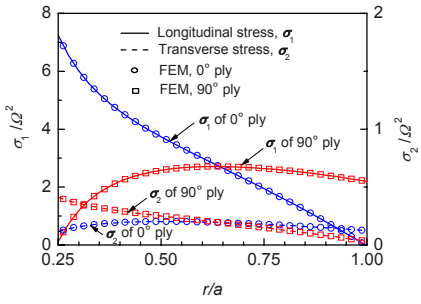

Fig. 4. Stresses in each layer of CFRP $[0/90]_S$ disk.

disks are considered ultimately failed when either fiber breakage or matrix failure occurs. The $[0/90]_S$ disk is considered failed when fiber breakage occurs since matrix failure in the $[0/90]_S$ disk does not imply ULF, and fiber breakage in the $[0/90]_S$ disk means no more load capacity in that direction. Another matrix cracking in the other layer after the first matrix cracking in one layer of the $[0/90]_S$ disk does not mean ULF and is regarded as second-ply failure (SPF). The failed lamina is replaced with a lamina with reduced stiffness. The ply discount method is used to reduce stiffness, i.e., $E_2 = 0$ and $G_{12} = 0$ for the failed lamina.

It is shown in Table 2 that the [0] disks have the highest allowable rotating speed in the aspect of FPF, whereas the $[0/90]_S$ disks have the lowest allowable rotating speed. However, the ULF should be estimated since failure of a lamina does not imply total failure of the laminate. Moreover, a single lamina plate is seldom used due to practical reasons. It could be said in the aspect of ULF that the $[0/90]_S$ GFRP disk has much higher maximum rotating speed than the other GFRP disks. It can be remarked that the matrix failure in the [0] and [90] GFRP disks makes their maximum rotation speed lower. However, in the case of the $[0/90]_S$ GFRP disk, the FPF is the matrix failure in the 90° layer. Following this FPF, the matrix failure in the 0° layer continues up to the ULF which is the fiber breakage in the 0° layer. In contrast to the results of the GFRP disks, the [0] CFRP disk has a bit higher maximum rotation speed than the $[0/90]_S$ CFRP disk. The matrix failure of the [0] CFRP disk would not occur prior to fiber breakage because the CFRP has much lower transverse stress and higher Y_t than the GFRP.

To study the effect of the number of 0° layers on the strength of the cross-ply laminate disk, the cross-ply ratio is defined as

$$M = \frac{i}{j} \tag{20}$$

where i and j are the total thickness of the 0° and 90° layers, respectively; they become the number of 0° and 90° layers if all the layers have an equal thickness as used in this paper. The cross-ply laminate disks studied in this paper have a stacking sequence $[0_i/90_j]_S$ where i and j are integer numbers from 0 to 10 with $i + j = 10$, keeping the laminate thickness h to 1.2 mm. The equations in the Appendix should be used in case of $\mu^2 = 9$ which corresponds to $[0/90_9]_S$ laminate with matrix failure in both 0° and 90° layers.

Fig. 5 shows the radial force resultant induced by rotation, N_r of the $[0_i/90_j]_S$ GFRP disk for the various cross-ply ratios. The unit of the rotating speed Ω is rad/s in the figures following hereafter. When $i = 10$, the distribution of N_r is shown to be similar to that of isotropic disk. A disk with $i = 10$ corresponds to the [0] disk where all fibers are oriented in the radial direction. The maximum value of N_r is lowest when $i = 0$. However, since a disk with $i = 0$ corresponds to the [90] disk in which only the matrix should sustain the radial loads, failure can occur at a low rotating speed. Therefore, a proper cross-ply ratio for maximum rotating speed should be found by strength analysis.

The in-plane circumferential force resultant induced by rotation, N_θ of the GFRP disk is shown in Fig. 6 for the various cross-ply ratios. It is found that the maximum value of N_θ can be reduced by increasing the cross-ply ratio. The maximum value of N_θ is lowest when $i = 10$. This is the case that only the matrix should resist the circumferential load.

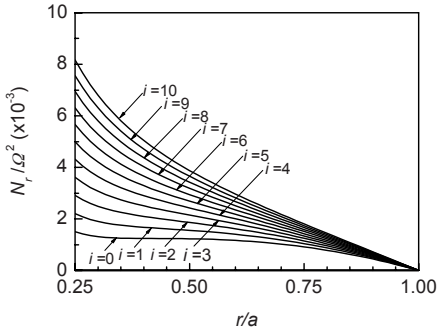

Fig. 5. Radial in-plane force N_r/Ω^2 of GFRP laminate disk for various cross-ply ratios.

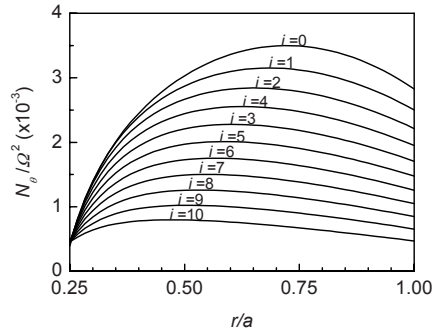

Fig. 6. Circumferential in-plane force N_θ/Ω^2 of GFRP laminate disk for various cross-ply ratios.

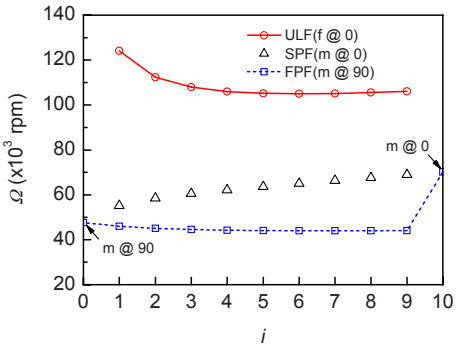

Fig. 7. Rotating speeds at failure of GFRP laminate disk.

The Tsai-Wu failure criterion is applied to the GFRP disk for the various cross-ply ratios in order to obtain the maximum rotating speeds as shown in Fig 7. Stresses in each layer for failure analysis are calculated by using Eqs. (1), (18) and (19) with N_r in Fig. 5 and N_θ in Fig. 6. The symbols square (□), triangle (△), and circle (○) in Fig. 7 denote the rotating speeds at which FPF, SPF (second-ply failure) and ULF occur, respectively. As can be observed in Fig. 7, all FPF's of the cross-ply laminate disks ($1 \le i \le 9$) are the matrix failure in the 90° layer (denoted by m@90). When $i = 0$, the matrix failure in the 90° layer is also initiated, corresponding to both FPF and ULF. On other hand, the matrix failure in the 0° layer (denoted by m@0) is both FPF and ULF when $i = 10$. The SPF occurs in the form of the matrix failure in the 0° layer when $1 \le i \le 9$. The equations in the Appendix are used to calculate the rotating speed for the ULF of the laminate with $i = 1$ in matrix failure in both 0° and 90° layers. Except for the single lamina disks, the ULF is the fiber breakage in the 0° layer. The maximum rotating speed of the $[0_i/90_j]_S$ GFRP disk is shown to be highest when $i = 1$. The results obtained illustrate that the cross-ply laminate GFRP disks can have much higher rotating speed than the single lamina GFRP disks.

Fig. 8 and Fig. 9 show N_r and N_θ of the $[0_i/90_j]_S$ CFRP disk for the various cross-ply ratios, respectively. At most of the cross-ply ratios, N_r is strictly decreasing, except for $i = 0$ and $i = 1$ at which N_r goes in a seesaw pattern as the radius increases. The distribution of N_θ for the CFRP disk shown in Fig. 9 is similar to that of the GFRP disk.

Fig. 10 illustrates the rotating speeds at which each failure of the $[0_i/90_j]_S$ CFRP disk occurs. As in the case of the GFRP disk, all FPF's of the cross-ply CFRP disks ($2 \le i \le 9$) are the matrix failure in the 90° layer. However, when $i = 10$, the FPF is the fiber breakage corresponding to the ULF instead of the matrix failure. The SPF occurs only at $i =$ 1, 2, 3 in the form of the matrix failure in the 0° layer while the SPF does not occur over $i = 4$. The ULF is the fiber breakage in the 0° layer except for $i = 0$. The $[0_i/90_j]_S$ CFRP disk has, in the aspect of ULF, the highest maximum rotating speed at $i = 1$ like the GFRP disk.

5. Conclusions

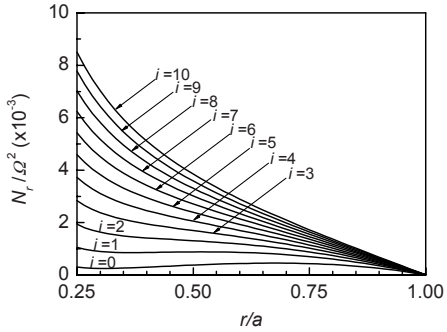

Fig. 8. Radial in-plane force N_r/Ω^2 of CFRP laminate disk for various cross-ply ratios.

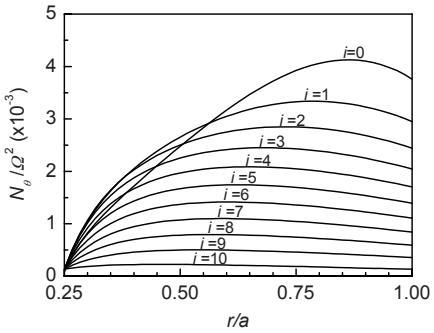

Fig. 9. Circumferential in-plane force N_θ/Ω^2 of CFRP laminate disk for various cross-ply ratios.

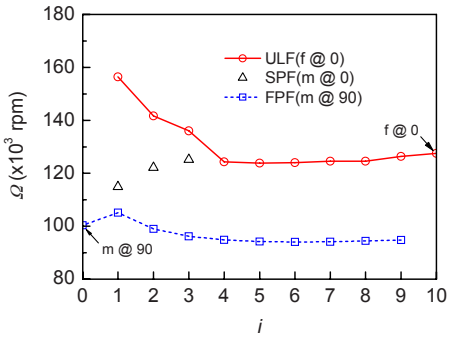

Fig. 10. Rotating speeds at failure of CFRP laminate disk.

Although the application of fiber-reinforced composite materials to rotating data storage disks such as CD, DVD, and HD has been known to increase the critical speeds by the present author, there has not been any research on the stress and vibration analysis of multidirectional laminated disks. In this paper, the close-form solutions for stress distribution of rotating multidirectional laminate disks are found. As an application of the present solutions, a failure analysis of the rotating cross-ply disks is performed based on the Tsai-Wu failure criterion, from which the maximum allowable speed is obtained.

Numerical examples applied to GFRP and CFRP cross-ply laminate disks with CD geometry show that the cross-ply laminate disk has much higher maximum rotating speed than the single lamina disk in the aspect of ULF. It can be concluded that the optimal cross-ply ratio for the ULF strength of rotating cross-ply disks is 1/9 among those considered in this paper. As a future work, the derived formulae for stresses will be used in the vibration analysis of rotating laminate disks to determine natural frequencies and critical speeds.

Appendix

The general solution in the case of $\mu^2 = 9$ can be written as

$$\bar{u}_r(r) = c_1 r^3 + c_2 r^{-3} - \frac{\rho h \Omega^2}{6A_{rr}} r^3 \ln r \,. \tag{A.1}$$

The coefficients satisfying the boundary conditions are

$$c_1 = \frac{\rho h \Omega^2}{6A_{rr}} \frac{e}{d}, \quad c_2 = \frac{\rho h \Omega^2}{6A_{rr}} \frac{f}{d} \tag{A.2}$$

where

$$e = [1 + (3+\eta)\ln a]a^3 b^{-3} + (3-\eta)a^{-3}b^3 \ln b$$
$$f = [1 + (3+\eta)\ln(a/b)]a^3 b^3,$$
$$d = (3+\eta)a^3 b^{-3} + (3-\eta)a^{-3}b^3 \,. \tag{A.3}$$

Substituting $\bar{u}_r(r)$ in Eq. (A1) into Eq. (9) gives

$$\frac{N_r}{\rho h \Omega^2} = (c_{r1} - 1)r^2 + c_{r2} r^{-4} - c_{r3} r^2 \ln r \,,$$
$$\frac{N_\theta}{\rho h \Omega^2} = (c_{\theta 1} - \eta)r^2 + c_{\theta 2} r^{-4} - c_{\theta 3} r^2 \ln r \tag{A.4}$$

where

$$c_{r1} = \frac{3+\eta}{6}\frac{e}{d}, \quad c_{r2} = \frac{3-\eta}{6}\frac{f}{d}, \quad c_{r3} = \frac{3+\eta}{6},$$
$$c_{\theta 1} = 3c_{r1}, \quad c_{\theta 2} = -3c_{r2}, \quad c_{\theta 2} = \frac{9+3\eta}{6} \,. \tag{A.5}$$

References

[1] S.-Y. Lee, J.-Y. Kim and S. Lim, Critical and flutter speeds of optical disks, *Microsystem Technologies*, 8 (2-3) (2002) 206-211.

[2] K.-N. Koo, Vibration analysis and critical speeds of polar orthotropic annular disks in rotation, *Composite Structures*, 76 (1-2) (2006) 67-72.

[3] C. I. Chang, A closed-form solution for an orthotropic rotating disk, *Journal of Applied Mechanics*, 41 (1) (1974) 1122-1123.

[4] S. Tang, Elastic stresses in rotating anisotropic disks, *International Journal of Mechanical Sciences*, 11 (6) (1969) 509-517.

[5] T. Y. Reddy and H. Srinath, Elastic stresses in a rotating anisotropic annular disk of variable thickness and variable density, *International Journal of Mechanical Sciences*, 16 (2) (1974) 85-89.

[6] G. Genta and M. Gola, The stress distribution in orthotropic rotating disks, *Journal of Applied Mechanics*, 48 (1981) 559-562.

[7] R. Jain, K. Ramachandra and K. R. Y. Simha, Singularity in rotating orthotropic discs and shells, *International Journal of Solids and Structures*, 37 (2000) 2035-2058.

[8] K.-N. Koo, In-plane stress analysis of rotating composite disks, *Journal of the Korean Society for Composite Materials*, 18 (4) (2005) 8-13.

Kyo-Nam Koo received his B.S. and M.S. degrees in Aerospace Engineering from Seoul National University, Korea, in 1987 and 1989, respectively. He then received his Ph.D. degree from Korea Advanced Institute of Science and Technology in 1994. Dr. Koo had worked with Korea Aerospace Research Institute for seven years after his education. He is currently a Professor at the Department of Aerospace Engineering at University of Ulsan in Korea since 2001. His research interests include composite materials, structural dynamics, finite element analysis, and aeroelasticity.